NANO: Brief Reports and Reviews
Vol. 12, No. 5 (2017) 1750062 (8 pages)

DOI: 10.1142/S179329201750062X

World Scientific
www.worldscientific.com

Analysis of Local Surface Plasmon Resonance in Multilayered Au/Ag/Graphene Nanoshells

Chao Liu*,§, Zhaoting Liu*, Jingwei Lv*, Tao Sun†, Qiang Liu*, Haiwei Mu* and Paul K. Chu‡

*School of Electronics Science, Northeast Petroleum University Daqing 163318, P. R. China

†Institute of Microelectronics, Agency of Science Technology and Research (A*STAR), Singapore 117685

‡Department of Physics and Materials Science City University of Hong Kong, Tat Chee Avenue, Kowloon Hong Kong, P. R. China

§msm-liu@126.com

Received 27 December 2016
Accepted 23 March 2017
Published 31 May 2017

The localized surface plasmon resonance (LSPR) properties of Au/Ag/graphene nanoshells are studied by discrete dipole approximation (DDA). The coupled resonance wavelengths show a remarkable dependence on the graphene thickness as well as refractive index of the surrounding medium. The resonance wavelengths of Au/Ag/graphene nanoshells red-shift as the thickness of the graphene layer is increased, when the radii of the Au core and Ag interlayer are 40 nm and 45 nm, respectively. Specifically, the longer wavelength red-shifts from 540 nm to 740 nm when the refractive index varies from 1.25 to 2.05.

Keywords: DDA; LSPR; Au/Ag/graphene; nanoshells.

1. Introduction

The strong interaction between light and nanoparticles has attracted considerable attention due to unique plasmonics, which is of great interest to nanophotonics.[1] Plasmonics is regarded as a prospective approach to realize light manipulation on the nanoscale mainly due to the capability of supporting localized surface plasmon resonance (LSPR). In general, LSPR refers to the ability of the conduction electrons in nanoparticles to oscillate collectively, resulting in concentration and enhancement of the electromagnetic energy surrounding the nanoparticles.[2] Owing to their characteristic LSPR, metal nanoparticles have been widely used in biosensing and imaging applications.

Traditionally, gold and silver are the preferred materials in the synthesis of LSPR nanoparticles[3–6] and both of them possess some merits and shortcomings. Although gold nanoparticles are easier to synthesize and have better biocompatibility as well as long-term stability, silver nanoparticles have advantages such as a more intense absorption band in surface-enhanced Ramon scattering and sensing applications. Up to date, much effort has been

devoted to the investigation of LSPR properties and electric field enhancement of gold and silver nanoparticles with various structures such as nanospheres,[7] nanorods[8] and nanoshells.[9,10] Among these nanostructures, the core/shell nanostructures based on Au and Ag have been demonstrated to significantly affect the LSPR properties in combination with other metals,[11,12] semiconductors[13–16] and magnetic materials.[17,18] As a result of the combined advantages and improved optical response,[19] Au/Ag bimetallic nanoparticles are attractive. The optical properties of spherical Au/Ag and Ag/Au core/shell nanoparticles have been studied by the extended Mie theory in the wavelength range between 300 nm and 650 nm.[20] Xu *et al.*[21] investigated the LSPR properties of core/shell nanostructures separated by a cavity and resonance cavity enhancement and new absorption bands were observed due to more interfaces and consequent plasmon coupling. In general, the LSPR spectra of nanoparticles exhibit size- and shape-dependent properties and the performance of nanoparticles can be optimized by controlling their shape and size on the nanometer scale.

With regard to metallic nanoshells, there is a great challenge to tune the operation wavelength due to limitations in modifying the permittivity and core–shell ratio. It is thus important to explore novel active optical materials to promote LSPR excitation. Recently, graphene has attracted much attention due to its extraordinary electronic, optical, magnetic, thermal and mechanical properties.[22] Graphene, a two-dimensional (2D) form of sp^2-hybridized carbon atoms arranged in six-membered rings, exhibits intriguing surface plasmon properties[23] and whose plasmonic resonance wavelengths are generally located in the range of visible light and infrared or even longer wavelength regions. A large number of studies have been performed for activating surface-enhanced Raman scattering in noble metal-graphene hybrids.[24–26] However, in spite of these attractive nanostructures, further efforts are needed to investigate three layers nanoshells with covering graphene outer layer.

In this study, the LSPR properties of Au/Ag/graphene core–shell nanoparticles are investigated by the discrete dipole approximation (DDA) method. The effects of the graphene thickness and refractive index of the surrounding medium on the LSPR properties of the nanoparticles are studied. Moreover, the electric field enhancement contour around the multilayered nanoshells is analyzed.

2. Theory

DDA is a powerful technique to study the scattering and absorption of electromagnetic waves by targets with arbitrary geometries.[27] Generally, the continuum target can be substituted by discrete dipoles as long as the dipole number N is large enough, whose positions and polarizabilities are denoted as $\mathbf{r}_j$ and $\alpha_j^{\mathrm{CM}}(i = 1, 2, \ldots)$. α_j^{CM} can be achieved by

$$\alpha_j^{\mathrm{CM}} = \frac{3d^3\varepsilon_j - 1}{4\pi\ \varepsilon_j + 2}, \tag{1}$$

where d is the interdipole spacing and ε_j is the dielectric function of the target material at location $\mathbf{r}_j$.

Analytical modification in Eq. (1) has been reportedly implemented in DDSCAT, the open source computational code of the DDA method.[28] DDSCAT creates a cubic lattice array of dipoles and assigns to each one a polarizability given by the lattice dispersion relation (LDR):

$$\alpha^{\mathrm{LDR}} \approx \frac{\alpha^{\mathrm{CM}}}{1 + (\alpha^{\mathrm{CM}}/d^3)[(b_1 + m^2 b_2 + m^2 b_3 S)(kd)^2 - (2/3)i(kd)^3]}, \tag{2}$$

$$b_1 = -1.891531, \quad b_2 = 0.1648469,$$
$$b_3 = -1.7700004, \quad S \equiv \sum_{j=1}^{3} (\hat{\alpha}_j \hat{e}_j)^2, \tag{3}$$

where $\hat{\alpha}$ and $\hat{e}$ are unit vectors defining the incident direction and the polarization state, S, b_1, b_2 and b_3 are the coefficients of the expansion to the third order in k to incorporate radiation effects.

The polarization vector is generated by the interaction between the arbitrary point dipole and local electric field $\mathbf{E}_j$ so that

$$\mathbf{P}_j = \alpha_j \mathbf{E}_j, \tag{4}$$

where α_j is the tensor of polarizability of the point dipole and $\mathbf{r}_j$ is the central position. $\mathbf{E}_j$ consists of the electric field $\mathbf{E}_{\mathrm{inc},j}$ at position j due to the incident plane wave and the electric field stimulated by $(N-1)$ other dipoles is as follows

$$\mathbf{E}_{\mathrm{inc},j} = \mathbf{E}_0 \exp i(\mathbf{k} \cdot \mathbf{r}_j - \omega t), \tag{5}$$

$$\mathbf{E}_j = \mathbf{E}_{\text{inc},j} - \sum_{k \neq j} \mathbf{A}_{jk}\mathbf{P}_k, \tag{6}$$

where $-\mathbf{A}_{jk}\mathbf{P}_k$ represent the contribution to the electric field at $\mathbf{r}_j$ that is due to the dipole $\mathbf{P}_k$ at position $\mathbf{r}_k$, including retardation effects. Each element $\mathbf{A}_{jk}$ is a 3×3 matrix

$$\mathbf{A}_{jk} = \frac{\exp(ikr_{jk})}{r_{jk}} \times \left[k^2(\hat{r}_{jk}\hat{r}_{jk} - \mathbf{1}_3) + \frac{ikr_{jk} - 1}{r_{jk}^2}(3\hat{r}_{jk}\hat{r}_{jk} - \mathbf{1}_3)\right], \quad j \neq k, \tag{7}$$

where $|\mathbf{k}| \equiv \omega/c$, $\mathbf{r}_{jk} \equiv |\mathbf{r}_j - \mathbf{r}_k|$, $\hat{r}_{jk} \equiv (\mathbf{r}_j - \mathbf{r}_k)/r_{jk}$, and $\mathbf{1}_3$ is the 3×3 identity matrix. Defining $\mathbf{A}_{jj} = \alpha_j^{-1}$ reduces the scattering problem to finding the polarizations $\mathbf{P}_j$ that can be briefly described as a set of $3N$ complex linear vector equations

$$\sum_{k=1}^{N} \mathbf{A}_{jk}\mathbf{P}_k = \mathbf{E}_{\text{inc},j}. \tag{8}$$

Once the polarization $\mathbf{P}_j$ is known, the absorption cross section of the entire grain is

$$C_{\text{abs}} = \frac{4\pi k}{|\mathbf{E}_0|^2} \sum_{j=1}^{N} \left\{ \text{Im}\left[\mathbf{P}_j \cdot (\alpha_j^{-1})^* \mathbf{P}_j^*\right] - \frac{2}{3}k^3 |\mathbf{P}_j|^2 \right\}. \tag{9}$$

The extinction cross section and extinction efficiency can be obtained by the optical theorem (7):

$$C_{\text{ext}} = \frac{4\pi k}{|\mathbf{E}_0|^2} \sum_{j=1}^{N} \text{Im}(\mathbf{E}_{\text{inc},j}^* \cdot \mathbf{P}_j), \tag{10}$$

$$Q_{\text{ext}} = \frac{C_{\text{ext}}}{\pi R^2}. \tag{11}$$

The isolated concentric Au/Ag/graphene core–shell nanoparticle is modeled as shown in Fig. 1. The Au core and multi-layered graphene shell are separated by Ag interlayers. For convenience of calculations, 1-nm thick graphene is ideally comprised of three single-atomic carbon layers in this simulation. The dielectric functions of the materials are obtained from Palik's handbook[29] and SOPRA N&K database.[30]

3. Results and Discussion

3.1. *Ag/graphene nanoshells*

Figure 2 shows the extinction spectra of the graphene-coated Ag nanoshells. Here, the radius of the Ag core ranges from 5 nm to 40 nm, the thickness of the graphene layer is maintained at 2 nm, and the refractive index (n) of the surrounding medium is kept at 1.33. Figure 2 shows that the extinction efficiency of the silver-graphene nanoshells increases gradually and the resonance wavelength is at approximately 425 nm when the Ag core radius is between 5 nm and 40 nm. It has been predicted by the Mie theory[31] that the resonance wavelength of a single Ag nanosphere is around

Fig. 1. Model of the core (Au)-Ag-shell (graphene) nanoshells.

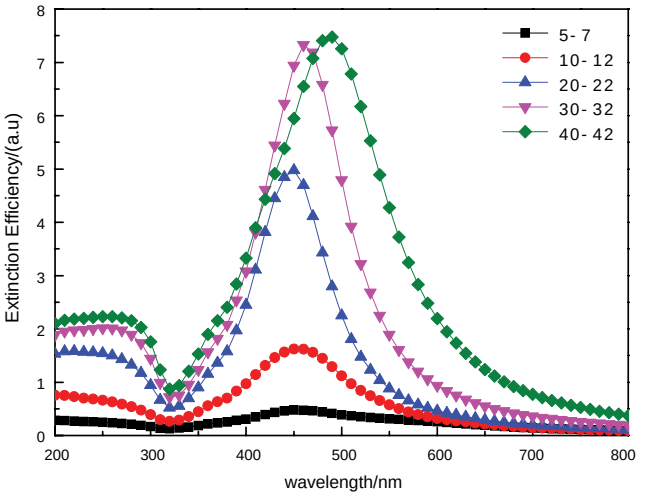

Fig. 2. Extinction spectra of the graphene-coated silver nanospheres.

370 nm and the intensity of the resonance band increases with the size of the Ag nanosphere increasing. Furthermore, in the case of a small nanosphere (< 40 nm), displacement of charges occurs homogeneously yielding a dipolar charge distribution on the surface. The shape of the silver nanosphere and the associated electron density determine only one proper resonance. The resonance wavelength of the silver-graphene nanoshell is larger than that of a single Ag nanosphere and it is attributed to the contribution of the interface between the silver core and graphene shell. Similar phenomena have been observed from Ag nanoparticles[32–34] and the resonance wavelengths vary between 380 nm and 500 nm.

3.2. *Au/Ag/graphene nanoshells*

In order to investigate the influence of the graphene layer thickness on the extinction spectra of multilayered nanoshells, Au/Ag nanoshells comprising the Au core and Ag shell are first considered. Figure 3 presents the extinction spectra of the Au/Ag nanoshells with different Au core radii. The radius of the Au core varies from 25 nm to 40 nm while the radius of Ag shell is kept at 45 nm. There are two resonance peaks in the extinction spectra corresponding to Ag shell quadrupole resonance of 370 nm and Au core dipole peak of 500 nm attributed to the Ag shell and Au core, respectively. The Au/Ag nanoshell has the strongest extinction intensity at 540.7 nm when the radius of the inner Au core and Ag shell are 40 nm and 45 nm, respectively. The intensity of the dipole and quadrupole resonance peaks decreases as the radius of the inner Au core increases. The dominant resonance peaks of the Au/Ag nanoshells shift towards longer wavelengths when the radius of the Au core increases from 25 nm to 40 nm.

Graphene is considered as an alternative coating layer for Ag- and Au-based LSPR as it has a very large surface-to-volume ratio which is expected to be beneficial to efficient adsorption of biomolecules compared to naked Au. Figure 4 shows the extinction spectra of the Au/Ag/graphene nanoshells with different graphene shell thicknesses. The radius of the inner Au core and Ag interlayer are 40 nm and 45 nm, respectively and the thickness of the graphene shell varies from 2 nm to 12 nm. Compared to the extinction spectra of the Au/Ag nanoshells, the Au/Ag/graphene nanoshells exhibit distinct variations in the extinction spectra. The dipole peak of the Au/Ag/graphene nanoshells is between 550 nm and 660 nm and larger than that of the Au/Ag nanoshells shown in Fig. 3 due to the graphene shells. Moreover, the dipole peak shift ($\Delta\lambda$) relative to 540.7 nm of the Au/Ag nanoshells in Fig. 3 depends on the graphene thickness for the dipole resonance peaks, as shown in Fig. 5. $\Delta\lambda$ exhibits a linear relationship with the thickness of the graphene layers and hence, the LSPR properties of the Au/Ag/graphene nanoshells can be tuned by adjusting the graphene layer thickness. In addition, the resonance wavelengths of the Au/Ag/graphene

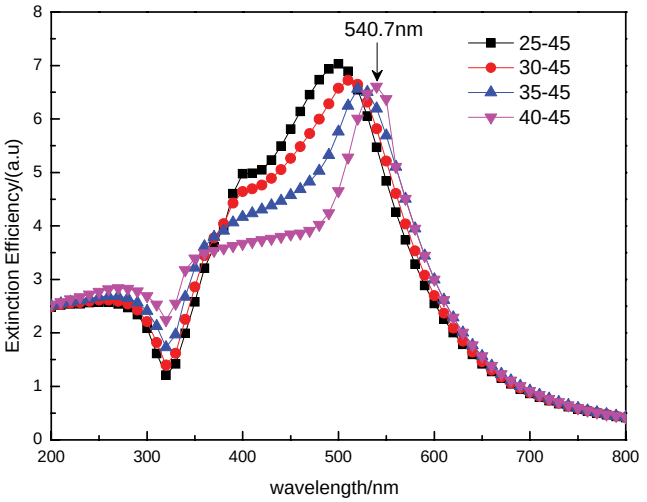

Fig. 3. Extinction spectra of the Ag-coated Au nanoshells with different Au core radii.

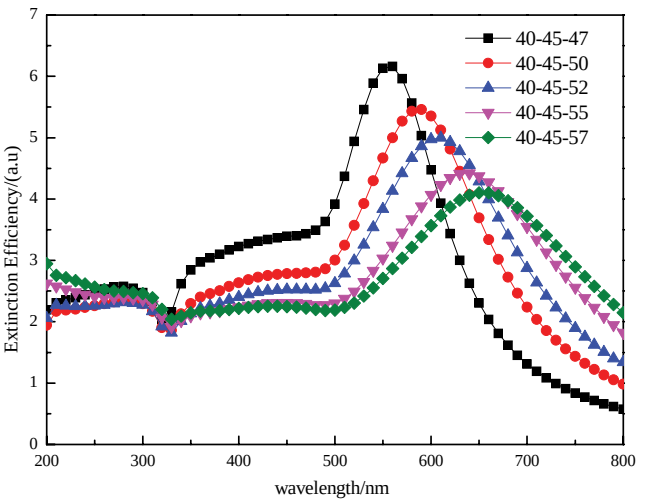

Fig. 4. Extinction spectra of the multilayered Au/Ag/graphene nanoshells with different layers of graphene.

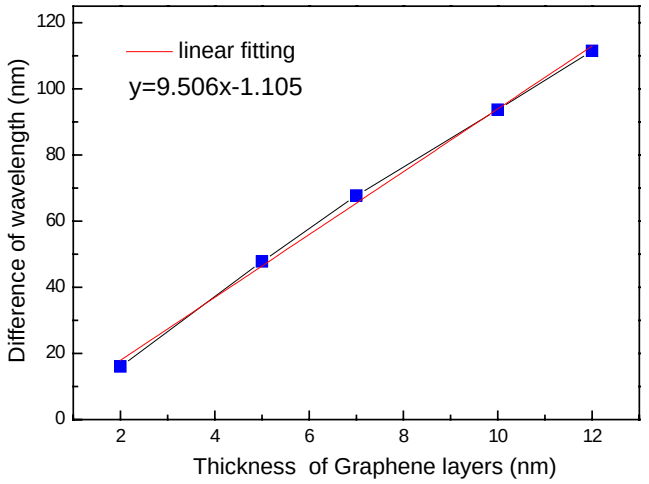

Fig. 5. Dependence of the dipole resonance wavelength shift ($\Delta\lambda$) relative to 540.7 nm of the Au/Ag bimetallic nanoshells with graphene thickness.

nanoshells red-shift and the extinction intensity of the nanoshells decreases with the graphene layer thickness arising from the large surface area, π conjugation structure of graphene, as well as strong absorption of light.[35]

The extinction spectra of the Au/Ag/graphene nanoshells for different refractive indexes of the surrounding medium are shown in Fig. 6. The radii of the inner Au core and Ag interlayer are 40 nm and 45 nm, respectively, and the Au/Ag nanoshells are coated with multilayered graphene with a thickness of 2 nm to form the Au/Ag/graphene nanoshells. The refractive indexes of the surrounding medium range from 1.25 to 2.05 in this calculation.

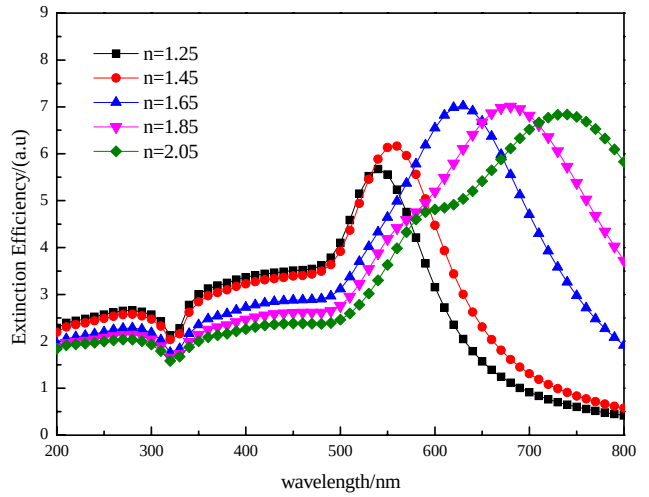

Fig. 6. Extinction spectra of the Au–Ag–graphene nanoshell as a function of the refractive index of the surrounding medium.

The resonance peaks of the Au/Ag/graphene move towards longer wavelengths and the intensity of the LSPR peaks increases as the refractive index of surrounding medium increases. The dipole peak red-shifts from 540 nm to 740 nm when the refractive index changes from 1.25 to 2.05. As the inner silver sphere is not in direct contact with the surrounding medium, the sensitivity of the multilayered structure to the surrounding medium depends on the outer graphene nanoshell and the interaction between the outer graphene nanoshell and inner silver core produces the red-shift.

Figure 7 displays the contours of the electric field enhancement of the Au/Ag/graphene nanoshells at different resonance wavelengths for a refractive index of $n = 2.05$. The radii of the Au core, Ag interlayer and graphene shell are 40 nm, 45 nm and 47 nm, respectively. In the simulation, the polarization direction is perpendicular to the propagation direction. At 270 nm, the electric field is concentrated in the region outside the Au/Ag/graphene multilayered nanoshell and Ag interlayer, whereas the electric fields in the inner Au core and graphene outer shell are small, as shown in Fig. 7(a). The electric field enhancement of the Au/Ag/graphene nanoshells at 450 nm is presented in Fig. 7(b). Owing to the different type of charges on the inner and outer surfaces of the Ag interlayer, there is always a strong electric field in the Ag interlayer. At 450 nm, the electric field at the interface between graphene and Ag is obviously stronger than that of the inner Au core.

Figure 7(c) describes the electric field enhancement with the quadrupole peak at 590 nm. The strong electric field spreads around the graphene outer shell but the fields in the Ag interlayer and Au inner core are very weak. The extinction peak at 590 nm originates from symmetric coupling between the bonding graphene shell plasmon mode and inner Ag plasmon. The electric field enhancement corresponding to the peak at 740 nm is displayed in Fig. 7(d). With respect to the Au/Ag/graphene nanoshells at 740 nm, the strongest enhancement appears on the surface of the outer graphene shell and a few nanometers outward, suggesting the dominant role of the outer graphene shell in the LSPR of the nanoshells. The Au/Ag/graphene nanoshell provides strong near-field enhancement in several regions, especially the near infrared region, and there are potential applications to plasmonics. In order to investigate the influence of the outer

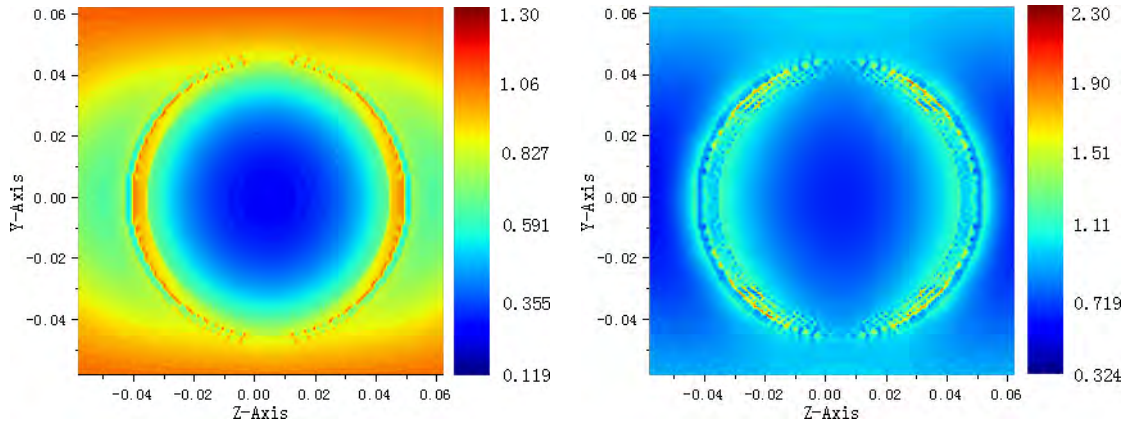

(a) Au/Ag/graphene, $\lambda = 270\,\text{nm}$

(b) Au/Ag/graphene, $\lambda = 450\,\text{nm}$

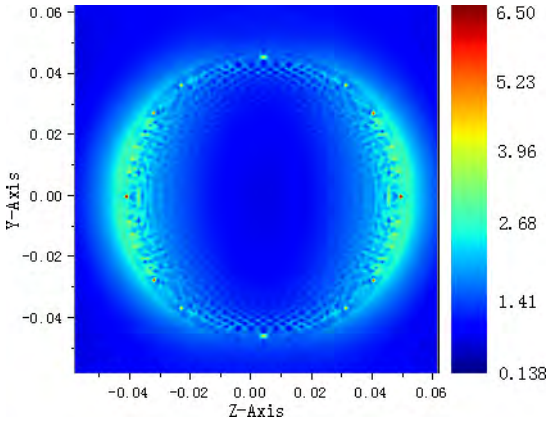

(c) Au/Ag/graphene, $\lambda = 590\,\text{nm}$

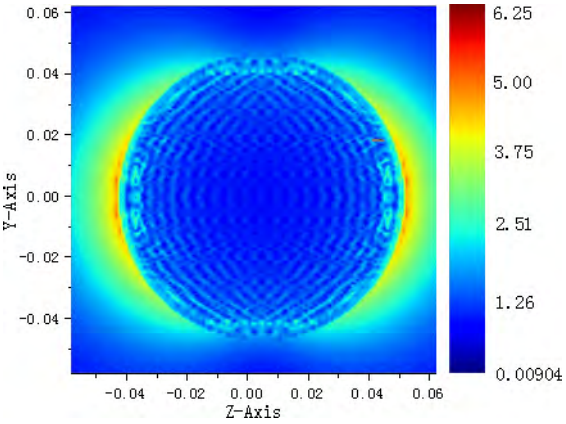

(d) Au/Ag/graphene, $\lambda = 740\,\text{nm}$

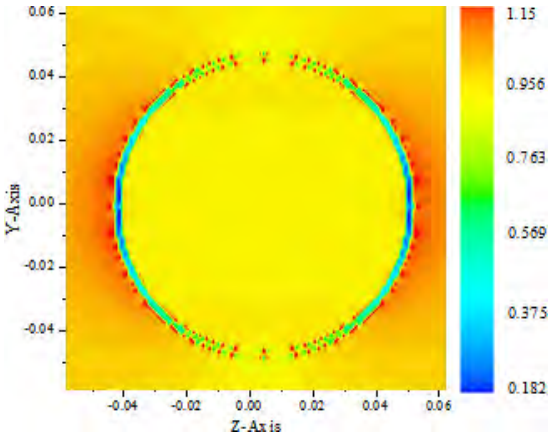

(e) Graphene cavity, $\lambda = 740\,\text{nm}$

Fig. 7. Electric field enhancement contours around the multilayered Au/Ag/graphene nanoshells illuminated at the plasmon resonance wavelength.

graphene shell on the electric field enhancement, Fig. 7(e) shows the electric field enhancement of hollow-graphene nanoshell with a thickness of 2 nm and inner radius of 45 nm at 740 nm. It can be seen that the strong electric field is concentrated on the inner surface and outside the graphene shell, which further verifies the dominant role of the outer graphene shell in the LSPR of the nanoshells at 740 nm.

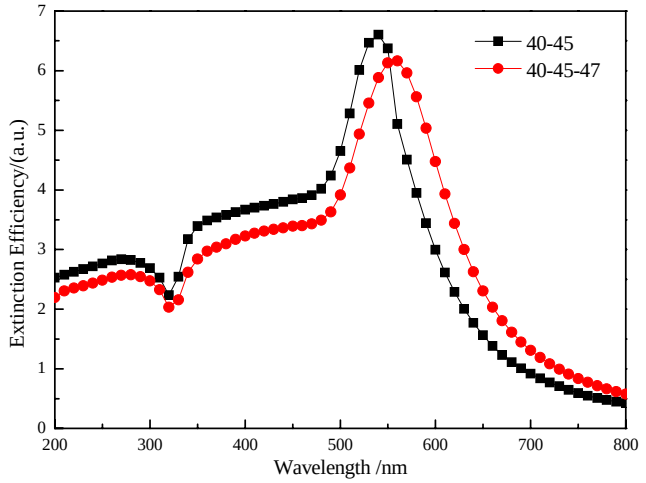

Fig. 8. Extinction spectra of the Au/Ag and Au/Ag/graphene nanoshells with the same refractive index of the surrounding medium $n = 1.33$.

To compare the optical properties of uncoated metal nanospheres, the extinction spectra of Au/Ag and Au/Ag/graphene nanoshells are investigated, as shown in Fig. 8. The radii of the inner Au core and Ag interlayer are 40 nm and 45 nm, respectively, and graphene is coated with a thickness of 2 nm to form the Au/Ag/graphene nanoshells. It can be seen from Fig. 8 that the longer wavelength at $\lambda = 540$ nm red-shifts as the thickness of graphene layers increases from 0 nm to 2 nm. The extinction efficiency of Au/Ag/graphene nanoshells is lower than that of Au/Ag nanoshells, which is mainly attributed to constant absorption capacity of graphene.

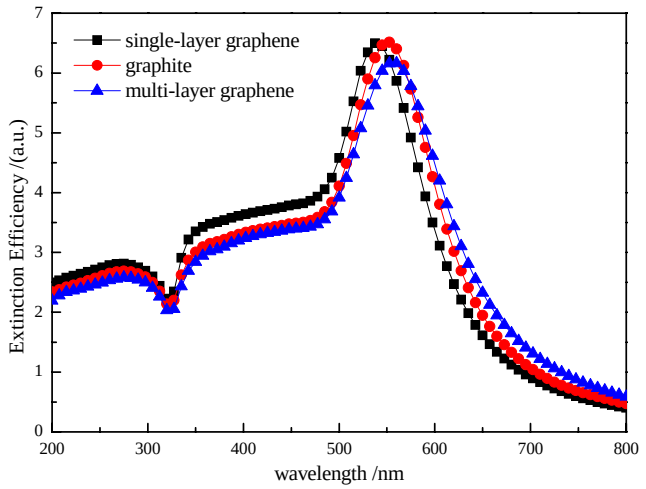

Fig. 9. Extinction spectra of the Au/Ag/graphite and Au/Ag/graphene nanoshells with the same refractive index of the surrounding medium $n = 1.33$.

In order to investigate the influence of outer shell material on extinction efficiency, the extinction spectra of the Au/Ag/graphite and Au/Ag/graphene nanoshells are plotted in Fig. 9. The refractive index of the surrounding medium is $n = 1.33$, and the thickness of the graphite, single-layer graphene and multi-layered graphene are 2 nm, 0.334 nm and 2 nm, respectively. In the spectrum of Au/Ag/multi-layer graphene nanoshells, a longer resonance wavelength exists at 560 nm, whereas the resonance wavelengths are observed at 552.5 nm and 537.5 nm for the Au/Ag/graphite and Au/Ag/single-layer graphene nanoshells, respectively. The results indicate that the resonance peak of Au/Ag/multi-layer graphene nanoshells are much more distinguishable than those of the nanoshells with graphite and single-layer graphene as the outer layer.

4. Conclusion

The extinction efficiency of the silver-graphene nanoshells increases gradually when the radius of the Ag core changes from 5 nm to 40 nm while the graphene thickness is maintained at 2 nm. The refractive index of the surrounding medium and outerlayer graphene thickness affect plasmon hybridization and LSPR shifts significantly and the outer graphene shell plays an important role in LSPR of the nanoshells. Inter-surface plasmonic coupling in the Au/Ag/graphene nanoshell can be tuned by changing the nanoshells, refractive index and thickness of the graphene shells. The Au/Ag/graphene nanoshells offer new opportunities to exploit and design plasmonic effects have potential applications in optics and biomedicine.

Acknowledgments

This work was supported by the National Natural Science Foundation of China (Grant No. 51474069), China Postdoctoral Science Foundation funded project (Grant No. 2016M591510), Natural Science Foundation of Heilongjiang Province (Grant No. E2016007), and City University of Hong Kong Applied Research (Grant No. 9667122).

References

1. L. B. William, D. Alain and W. E. Thomas, *Nature* **424**, 824 (2003).

2. N. Cecilia, *J. Phys. Chem. C* **111**, 3806 (2007).
3. C. Sönnichsen and A. P. Alivisatos, *Nano Lett.* **5**, 301 (2005).
4. G. Raschke, S. Brogl, A. S. Susha, A. L. Rogach, T. A. Klar, J. Feldmann, B. Fieres, N. Petkov, T. Bein, A. Nichtl and K. Kurzinger, *Nano Lett.* **4**, 1853 (2004).
5. A. D. McFarland and R. P. V. Duyne, *Nano Lett.* **3**, 1057 (2003).
6. H. Xu and M. Käll, *Phys. Rev. Lett.* **89**, 246802 (2002).
7. S. Raza, N. Stenger, S. Kadkhodazadeh, S. V. Fischer, N. Kostesha, A. P. Jauho, A. Burrows, M. Wubs and N. A. Mortensen, *Nanophotonics* **2**, 131 (2013).
8. E. K. Payne, K. L. Shuford, S. Park, C. S. George and C. A. Mirkin, *J. Phys. Chem. B* **110**, 2150 (2010).
9. J. T. Zhang, Y. Tang, K. Lee and M. Ouyang, *Science* **327**, 1634 (2010).
10. Y. H. Song, J. S. Luo, Y. Yi, K. Li, X. L. Tan, B. C. Luo, X. B. Xu and H. Lei, *Chem. Phys. Lett.* **614**, 21 (2014).
11. J. Tuaillon-Combes, E. Bernstein, O. Boisron and P. Mélinon, *Chem. Phys. Lett.* **564**, 65 (2013).
12. F. Bao, J. Li, B. Ren, J. Yao, R. Gu and Z. Tian, *J. Phys. Chem. C* **112**, 345 (2008).
13. S. V. Kahane, V. Sudarsan, S. Mahamuni and J. Lumin, **147**, 353 (2014).
14. T. Yang, W. Chen, Y. Hsu, K. Wei, T. Lin and T. Lin, *J. Phys. Chem. C* **114**, 11414 (2010).
15. V. P. Zhdanov and B. Kasemo, *Chem. Phys. Lett.* **524**, 16 (2012).
16. N. Kumar, V. K. Komarala and V. Dutta, *Chem. Eng.* **236**, 66 (2014).
17. S. Ramadurgam and C. Yang, *Sci. Rep.* **4**, 4931 (2014).
18. D. Llamosa Pérez, A. Espinosa, L. Martínez, E. Román, C. Ballesteros, A. Mayoral, M. García-Hernández and Y. Huttel, *J. Phys. Chem. C* **117**, 3101 (2013).
19. D. Wu, X. Xu and X. Liu, *J. Chem. Phys.* **129**, 074711 (2008).
20. V. K. Pustovalov, L. G. Astafyeva and W. Fritzsche, *Plasmonics* **7**, 469 (2012).
21. X. B. Xu, Z. Yi, X. B. Li, Y. Y. Wang, X. Geng, J. S. Luo, B. C. Luo, Y. G. Yi and Y. J. Tang, *J. Phys. Chem. C* **116**, 24046 (2012).
22. K. S. Novoselov, A. K. Geim, S. V. Morozov, D. Jiang, Y. Zhang and S. V. Dubonos, *Science* **306**, 666 (2004).
23. L. M. Tong, H. Wei, S. P. Zhang and H. X. Xu, *Sensors* **14**, 7959 (2014).
24. J. Li and C. Liu, *Eur. J. Inorg. Chem.* **8**, 1244 (2010).
25. Y. Liu, Y. Hu and J. Zhang, *J. Phys. Chem. C* **118**, 8993 (2014).
26. V. Amendola, *Phys. Chem. Chem. Phys.* **18**, 2230 (2016).
27. B. T. Draine and P. J. Flatau, *J. Opt. Soc. Am. A* **11**, 1491 (1994).
28. M. A. Yurkin and A. G. Hoekstra, *J. Quant. Spectrosc. Radiat. Transfer* **106**, 558 (2007).
29. E. D. Palik, *Handbook of Optical Constants of Solids* (Academic Press, New York, 1985).
30. SOPRA N&K Database, Available at www.refractiveindex.info.
31. K. L. Kelly, E. Coronado, L. L. Zhao and G. C. Schatz, *J. Phys. Chem. B* **107**, 668 (2003).
32. M. H. Lee, P. J. Dobson and B. Cantor, *Thin Solid Films* **219**, 199 (1992).
33. G. Xu, M. Tazawa, P. Jin and S. Nakao, *Appl. Phys. A* **80**, 1535 (2005).
34. R. Brahma and M. G. Krishna, *Nucl. Instrum. Meth. B* **266**, 1493 (2008).
35. J. Henri, He. Y, N. Granqvist and Z. P. Sun, *Optica* **3**, 151 (2016).